

Parameter studies for REXI

Martin Schreiber <M.Schreiber@exeter.ac.uk>
et al.

September 28, 2015

This document is on results for the REXI (In this work, we refer to REXI as described in [2][3]) and is based on the linear formulation of the SWE only. The main focus for creating this document were questions on the dependency of the REXI parameters h and M on the given scenarios described by the linear operator L and the initial conditions.

Several benchmarks are executed to evaluate these dependencies of the REXI parameters on scenarios representative for geophysical flows.

For sake of reproducibility, the benchmarks are given by (benchmark: [directory name]).

1 Benchmark scenario description

1.1 Equations

We analyze the behavior of REXI based on parameter studies of the linear part

$$L(U) := \begin{pmatrix} 0 & -\eta_0 \partial_x & -\eta_0 \partial_y \\ -g \partial_x & 0 & f \\ -g \partial_y & -f & 0 \end{pmatrix} U$$

of the SWE (see [1], note that the sign is inverted) with

$$U_t = \epsilon L(U)$$

with

$$U := (h, u, v)^T.$$

If not otherwise stated, we set $\epsilon = g = \eta_0 = f = 1$ and $\Omega = [0; 1]^2$.

1.2 Abbreviations

We give a brief overview of the used abbreviations for the parameter studies:

Symbol	Description
h	REXI parameter specifying the sampling accuracy
M	REXI parameter related to the number of poles
NxN	Resolution of simulation domain
τ	Time step size for REXI
dt	Time step size for REXI (identical to τ in this work)
DT	Overall simulation time
nT	Number of time steps
W	Parameter related to the number of waves in the initial conditions

1.3 Initial conditions

We consider the following initial conditions

1.3.1 Scenario “Gaussian” (Default)

If not otherwise stated, we use the Gaussian function

$$\begin{aligned}\eta(x, y) &:= \eta_0 + e^{-50(x^2+y^2)} \\ u(x, y) &:= 0 \\ v(x, y) &:= 0\end{aligned}$$

as initial conditions and use zero values for initial velocity conditions.

1.3.2 Scenario “Waves”

We also evaluate the following initial parameter from [2]:

$$\begin{aligned}h(x, y) &:= \sin(6\pi x)\cos(4\pi y) - \frac{1}{5}\cos(4\pi x)\sin(2\pi y) + \eta_0 \\ u(x, y) &:= \cos(6\pi x)\cos(4\pi y) - 4\sin(6\pi x)\sin(4\pi y) \\ v(x, y) &:= \cos(6\pi x)\cos(6\pi y)\end{aligned}$$

1.3.3 Scenario “Frequencies”

For testing different frequencies in the initial conditions, we also introduce additional frequencies via the parameter W by setting

$$\begin{aligned}fx &:= \pi \cdot x \cdot W \\ fy &:= \pi \cdot y \cdot W\end{aligned}$$

and use the following initial conditions:

$$\begin{aligned}h(x, y) &:= \sin(2fx)\cos(2fy) - \frac{1}{5}\cos(2fx)\sin(4fy) + \eta_0 \\ u(x, y) &:= \cos(4fx)\cos(2fy) \\ v(x, y) &:= \cos(2fx)\cos(4fy)\end{aligned}$$

1.4 Discretization in time

A Runge-Kutta time stepping method of 4-th order is used if appropriate. E.g. RK4 is not used for REXI, but for the other methods discussed in the next section.

1.5 Solvers and their discretization in space

The tests are based on different implementations in space:

1.5.1 Used derivatives

The derivatives in the linear operator L can be based on

- (FDderiv) Finite difference methods (e.g. a $[-1, 0, 1]$ stencil) or
- (SPderiv) computing the derivative via the spectral basis functions ($\frac{d}{dx}e^{ixj2\pi}$).

1.5.2 Realization of operator

Derivatives can be expressed either in

- (Cop) Cartesian space via a stencil computation (expensive in Cartesian space) or
- (Sop) Spectral (Fourier) space via a spectral convolution (element-wise multiplication and hence very cheap in spectral space).

1.5.3 Grid alignment

- (A-grid): All conserved quantities are placed at the cell center
- (C-grid): The potential is placed at the cell center and the velocity components at the cell edges.
Furthermore, computations are based on the vector invariant formulation.

1.5.4 REXI

There is only one REXI implementation considered, but with different parameters which are discussed below.

1.6 REXI

The REXI approach allows testing different parameters. In this work, we analyze the accuracy of REXI, based on the parameters h and M , see [3] for their description. The approximation is then given by a sum over a system of independent systems of equations to be solved:

$$e^{\tau L} \approx \sum_{n=0}^N \frac{\gamma_n^{Re}}{\tau L + \alpha_n} \quad (1)$$

We denote the result $U'(\tau)$ of the REXI approach by

$$U'(\tau) := REXI(U(0), \tau, h, M)$$

with U the solution at $t = 0$, the parameter τ the size of the large time step, h the sampling interval size and M related to the number of poles $K + M + 1$ used to compute REXI to L .

1.7 Error norm

We use the RMS error norm

$$RMS(f) := \sqrt{\frac{\sum_{\vec{x}} (f_{\vec{x}} - \tilde{f}_{\vec{x}})^2}{\prod_i N_i}}$$

based on a discrete computed solution $f_{\vec{x}}$ for the points given by $\vec{x}_i \in \{0, 1, \dots, \vec{N}_i\}$, the reference solution given by $\tilde{f}(\vec{x})$ and with each component in \vec{N} giving the resolution. In this work we only compare the RMS to the height η .

2 Analytical benchmark results

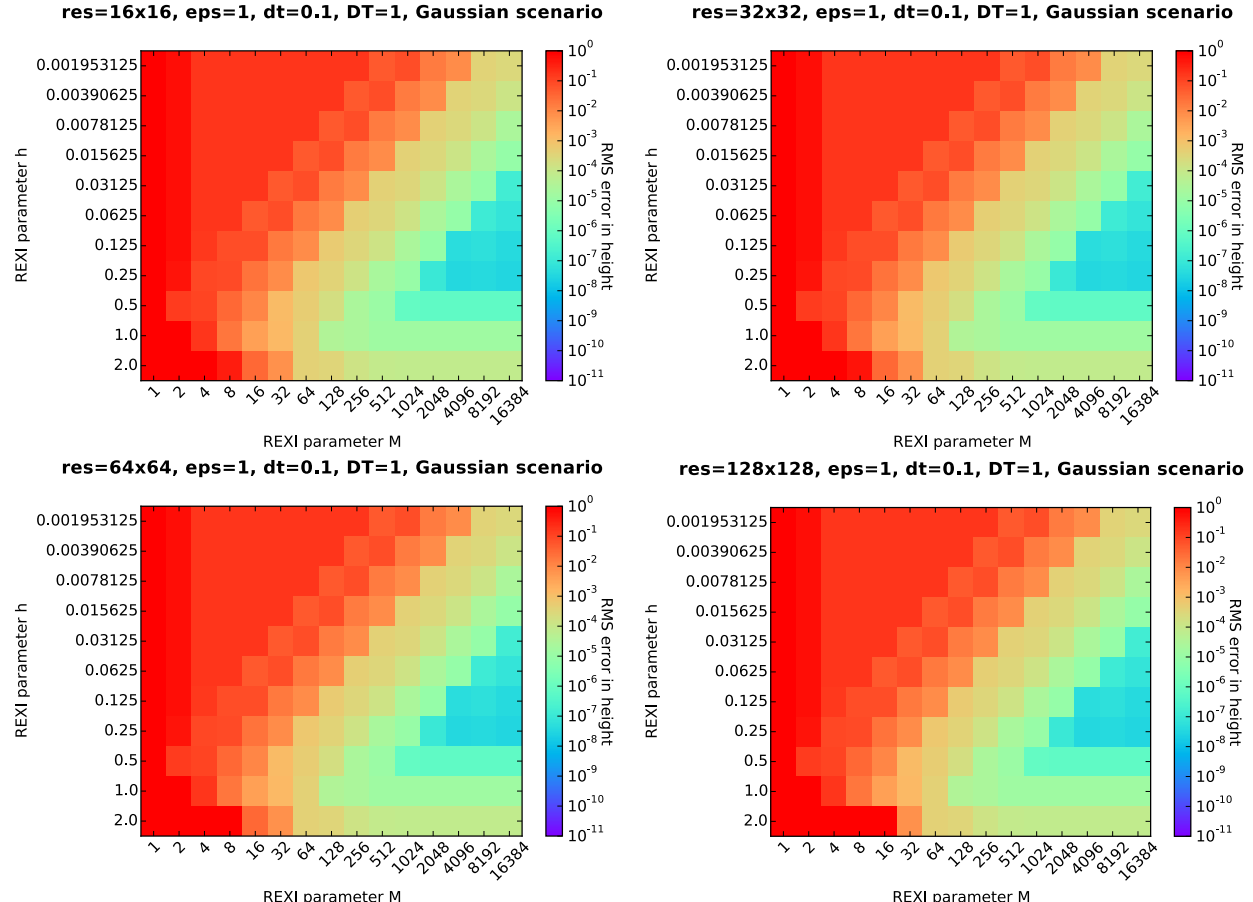
2.1 Study for REXI parameters h and M

(benchmark folder: 2015_09_04_search_h_M)

We first search for an optimal choice of h and M values. h is a value which only relates to the accuracy of the REXI approximation and M relates to the accuracy, as well as to the computational workload which has to be invested for the REXI approach. We execute the simulation for an overall simulation time of $DT := 1$ second and use a time step size for REXI of $dt := 0.1$. Hence, 10 time steps with REXI are executed. The results are given based on the computation of the RMS error on the height η .

2.1.1 Different resolutions

We first conduct a parameter study for different resolutions



We can observe a (blue-colored) triangle with high-accurate solutions of $O(10^{-6})$. This optimal triangle area for a given numerical accuracy e can be described by

$$A_{(M,h)} := \{(M,h) | Mh > C(e), h < 0.5\}$$

with $C := 1024$ for an accuracy $\approx 10^{-7}$.

We account for the diagonal edge at $Mh = \text{const.}$ by h specifying the sampling interval and M the sampling nodes. If a smaller value of h results in an oversampling of the frequency, more poles M have to be used to accurately cover the approximation of the solution. Since we should try to minimize M as far as possible, we can determine a particular best-investment for M at the left lower corner of the triangle area by choosing $h \in [0.125, 0.25]$.

We define such an optimal choice of h and M as the sweetspot for a given numeric solution $U'(t + \tau, h, M) := \text{REXI}(U(t), \tau, h, M)$ and a given numerical error threshold. We then search for parameters (M, h) which keep the error below a certain error threshold e and minimize the number of poles directly related to M . Then, this sweetspot is given by

$$S(h, M) := \min_M \min_h (\text{rms}(U'(t + \tau, h, M) - U(t\tau)) < e)$$

for the optimal choice of the parameters (h, M) .

2.1.2 Dependency of h and M on different resolutions N

Next, we test if both parameter changes for different resolutions (see above) and we can observe, that h can be fixed and we use $h := 0.2$ if not otherwise stated.

For these conducted benchmarks, a change in resolution did not significantly change the results for selected parameters h and M . Here, we like to mention, that this independency depends on the solver for $(L + \alpha)^{-1}$ and refer to Section 2.4.

2.1.3 Summary

REXI parameter	Observation
h	Optimum given at $h := 0.2$
M	Independent to the resolution

Given a desired numerical accuracy ϵ and with $h := 0.2$ assumed to be constant, the optimal parameters M is given by

$$M := \frac{C(\epsilon)}{h}. \quad (2)$$

2.2 Testing for different ϵ

(benchmark folder: 2015_08_30_search_epsilons, 2015_09_03_search_epsilons, 2015_09_03_search_epsilons_b)

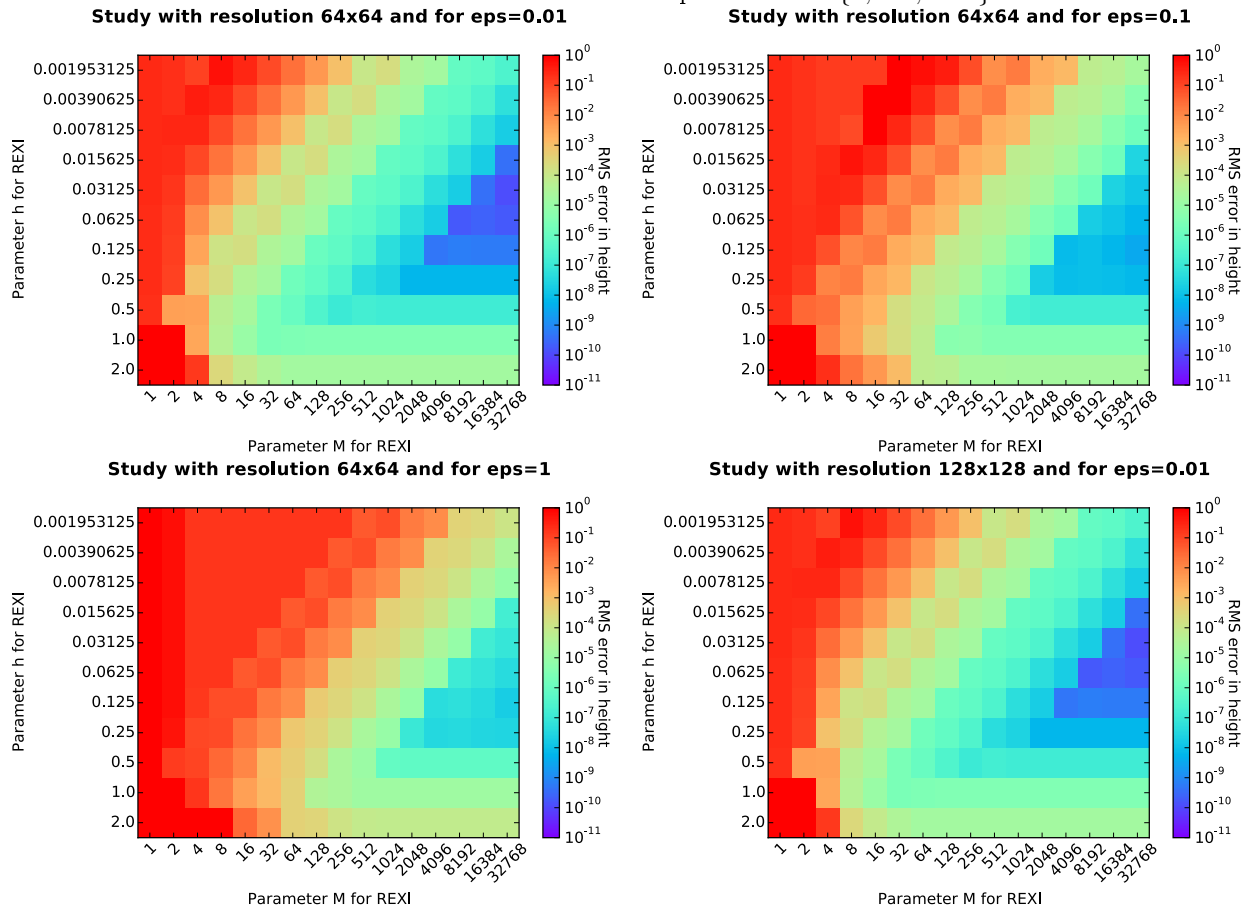
The REXI approach should hold for all the possible regimes of atmospheric constellations. Therefore, we generalize our formulation with ϵ

$$U_t = \epsilon L(U)$$

which we realize by setting $g = \eta_0 = f = \epsilon$ in our simulations.

2.2.1 Studies for $\epsilon := \{1, 0.1, 0.01\}$

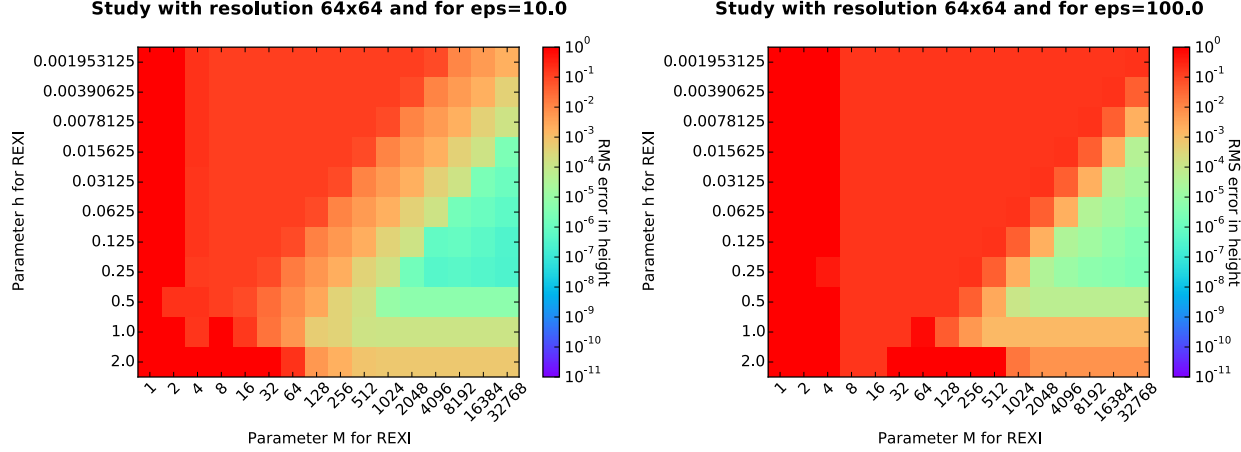
We fix our test resolution to 64^2 for this evaluation and show plots for $\epsilon := \{1, 0.1, 0.01\}$:



For a decreasing ϵ , we can see that the previously clear optimal parameters for (h, M) are now getting more diffusive. To see if the parameters (h, M) depend on the resolution, we added a plot for benchmarks with the resolution 128^2 and $\epsilon := 0.01$, see right bottom in the figures above. We can see, that the parameters of the REXI approach are again independent to the resolution for this scenario.

2.2.2 Studies for $\epsilon := \{10, 100\}$

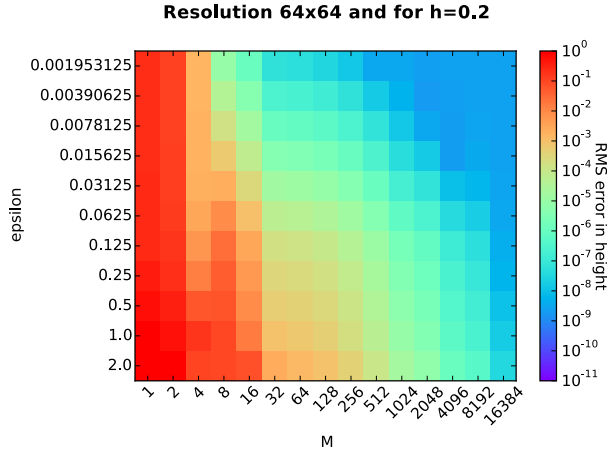
Since the borders got more diffusive for $\epsilon \ll 1$, we expect a sharp border for $\epsilon \gg 1$ which we evaluate next for sake of curiosity:



However, we don't see an increase in diffusiveness. But we can observe, that the solution area $A_{(M,h)}$ is shifted to the right side. Hence, for larger ϵ values (this increases the stiffness of the problem), we also have to increase M . We observe again, that the solution area $A_{(M,h)}$ still seems to be independent to the choice of $h \approx 0.2$.

2.2.3 Dependency of M to ϵ

To determine the dependency of M to ϵ , we finally executed a parameter study by setting $h := 0.2$ and with variables ϵ and M . Here, we keep the simulated time limited to $dT := 1$ and use a REXI timestep size of $dt := 0.1$.



We can see a linear dependency of M to ϵ in the range of $\epsilon \in [0.01; 1]$.

2.2.4 Summary

Regarding the results from Section 2.2.3, the REXI parameter M is proportional to ϵ : The larger the ϵ , the more poles have to be used for an approximation of sufficient accuracy. In combination with Eq. (2), we can extend the formula for automatically determining M to

$$M := \frac{C(\epsilon)\epsilon}{h}. \quad (3)$$

This dependency to ϵ gets more obvious with a straight-forward EV decomposition of L :

$$U(t) := e^{\epsilon t L} U(0) := \Sigma \Lambda \Sigma^{-1} U(0) = \Sigma \begin{bmatrix} e^{\epsilon t \lambda_0} & \\ & e^{\epsilon t \lambda_n} \end{bmatrix} \Sigma^{-1} U(0) = \Sigma e^{\epsilon t \Lambda} \Sigma^{-1} U(0)$$

with imaginary eigenvalues λ_i as the diagonal in Λ . Therefore, larger values of ϵ also lead to faster oscillations in the solution. Therefore, more poles have to be invested to capture these frequencies which is specified by M .

2.3 Study for REXI parameter M and resolution $N \times N$

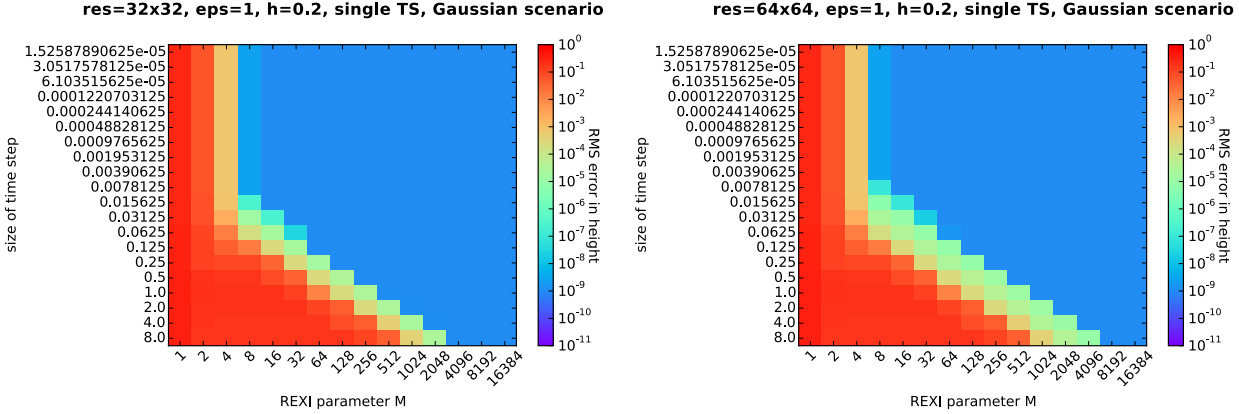
We start by evaluating the dependency of the REXI parameter M to the resolution $N \times N$ by a single time step. We again set $h := 0.2$ for these benchmarks and evaluate the dependency with the initial conditions described in Section (1.3).

2.3.1 Single time step

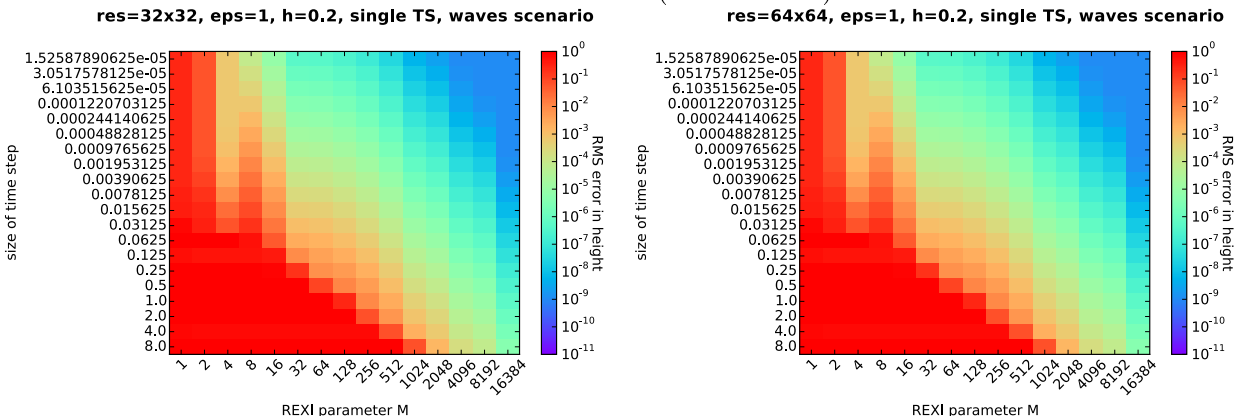
(benchmark: 2015_09_04_increasing_dt_single_timestep_s1, 2015_09_04_increasing_dt_single_timestep_s5)

The first tests are performed with a single time step and varying time step size.

We first have a look on the results for the Gaussian initial conditions:



We can observe, that there is indeed a dependency on the used resolution. However, this can be induced by using zero-valued velocity components as initial conditions. Therefore, we further evaluate this with initial conditions with non-zero velocities based on the wave initial conditions (see Sec. 1.3.2):

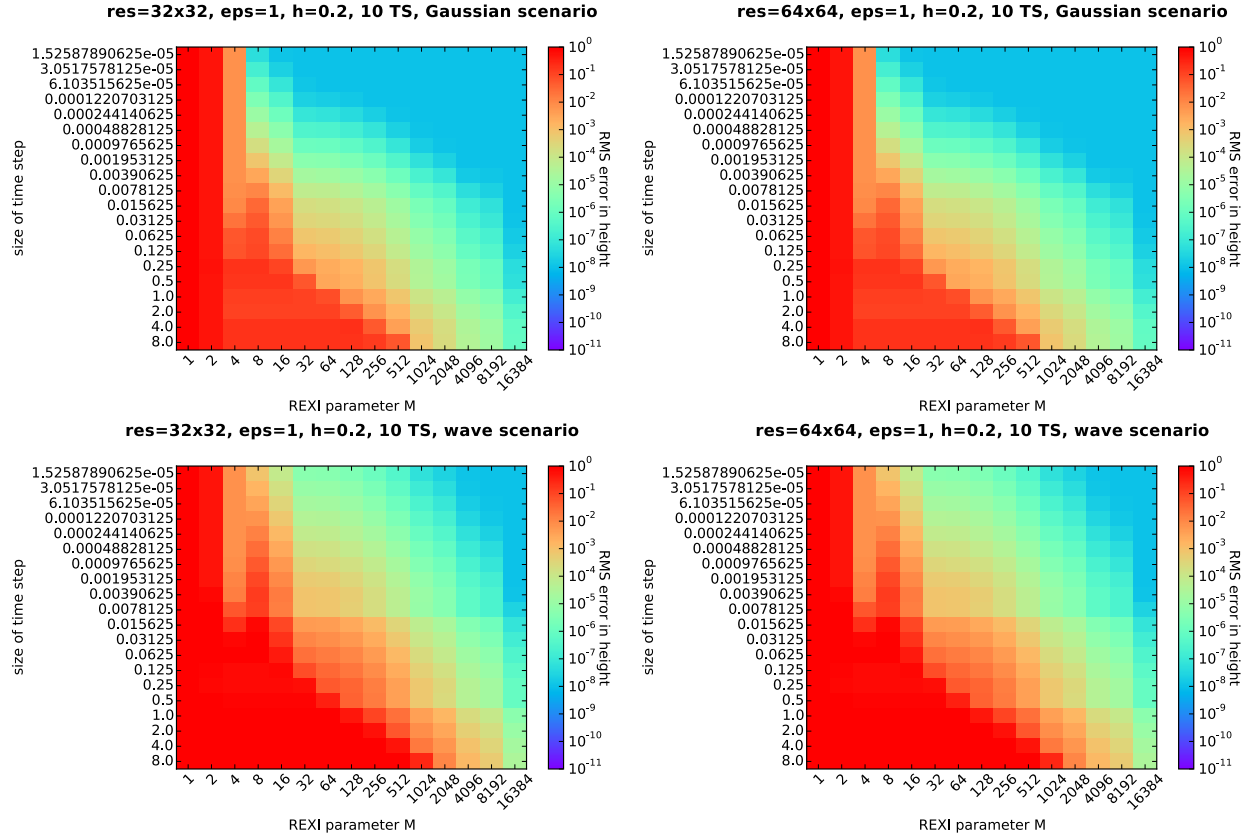


Here, we can observe that the accuracy of the solution again is independent to the resolution. An increasing time step size dt shows a linear dependency of M on dt .

2.3.2 Multiple time steps

(benchmark: 2015_09_04_increasing_dt_10_timesteps_s1, 2015_09_04_increasing_dt_10_timesteps_s5)

Next, we analyze the accuracy over multiple time steps with the Gaussian and Waves as initial conditions:

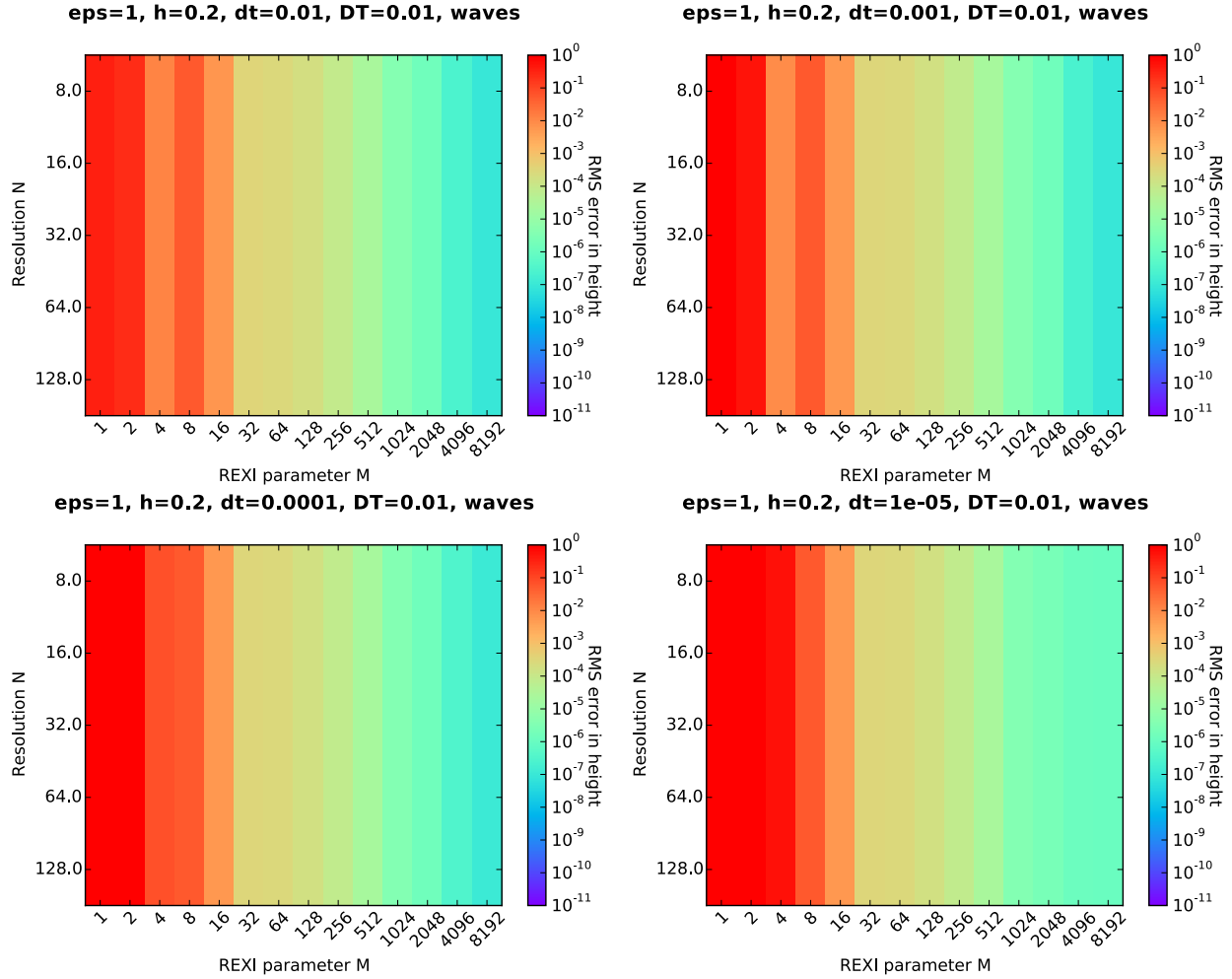


We can again observe, that the results show an independence to the resolution. Again, an increasing time step size dt results in a linear increase of M .

2.3.3 Different time step sizes over varying resolution N and M

(benchmark: 2015_09_04_study_N_M_small_ts)

The independence to the resolution can be caused by the large time step size dominating the error. To check that the error in time is not dominating (which would explain the independence of M to the resolution), we further analyze the error with very small time step sizes dt , varying M and varying resolution N :



For these small time step sizes, we can observe, that the change in resolution still does not result in any change regarding the parameter M depending on the resolution N .

2.3.4 Conclusion

An increasing time step size dt requires a linear increase of M . Therefore, we extend Equation (3) with dt .

$$M := \frac{dt C(e)}{h e}. \quad (4)$$

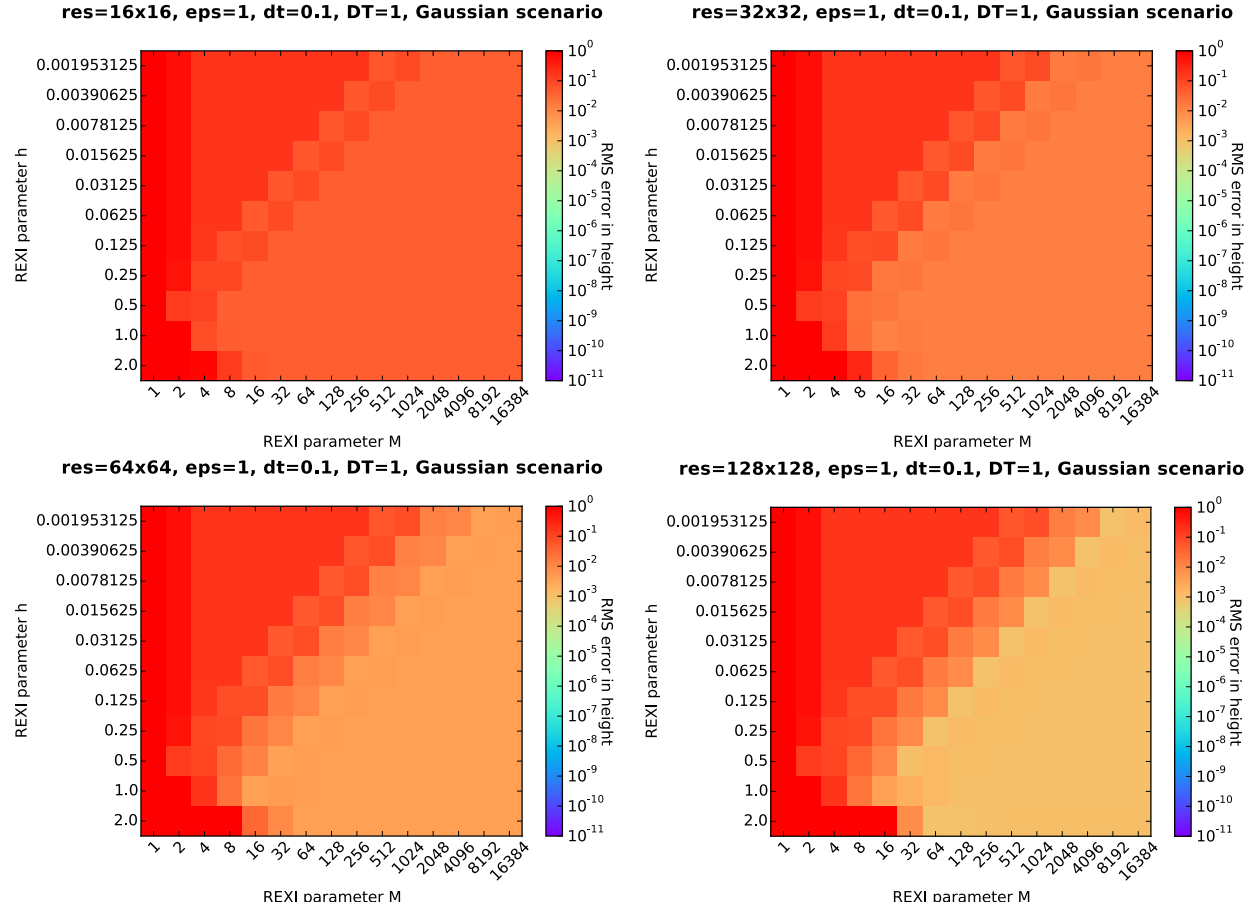
2.4 Finite-difference-based solution for $(\tau L - \alpha)^{-1}$

Since we use a spectral solver to solve for $(\tau L - \alpha)^{-1}$, this can be the reason of M being independent to the resolution M . Therefore, we run tests with an alternative solver in spectral space (to avoid implementing time-consuming alternative solvers): One which does not setup the derivative operator in spectral space (e.g. based on $\frac{\partial}{\partial x} e^{ixk} \tilde{u}(k) = ike^{ixk} \tilde{u}(k)$), but one which is based on a finite difference operator (e.g. $\frac{\partial}{\partial x} u(x) \approx \frac{u_{x+h} - u_{x-h}}{2h}$) specified in Cartesian space (see also Section 1.5.1), but applied as a folding operation in Fourier space.

Note, that despite we are using the Fourier space to solve this, the results are representative for the solution which would be computed with alternative solvers such as based on an LU decomposition or iterative solvers.

2.4.1 Studies for varying h and M

(benchmark: 2015_09_07_search_h_M_finite_differences)



For the 16^2 resolution, we like to mention that the initial conditions are barely captured by this resolution. Compared to computing $(L + \alpha)^{-1}$ with spectral methods,

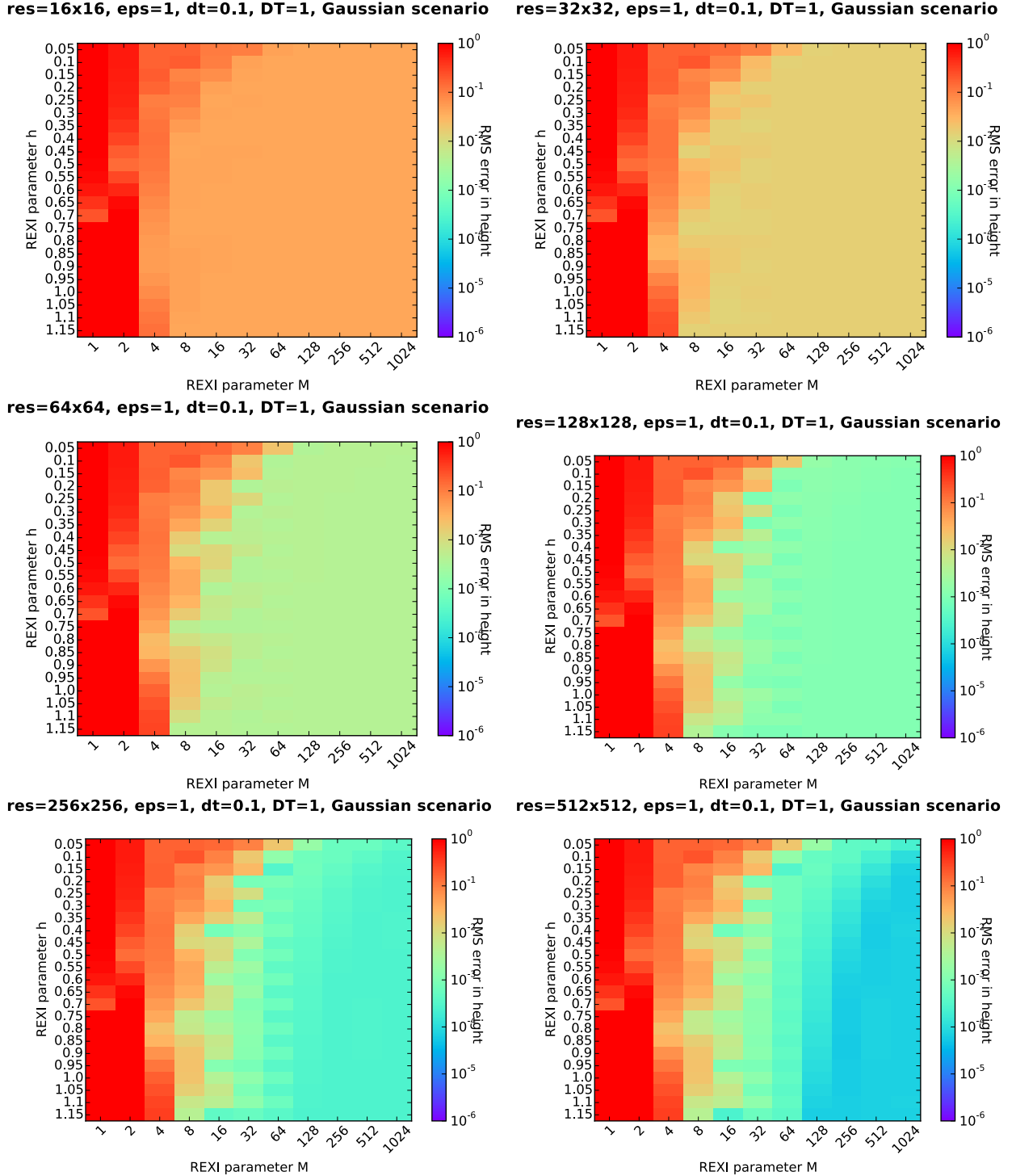
- Accuracy: We observe now a significantly reduced accuracy
- Optimal solution area: We can observe a similar “triangular”-shaped solution area. However, the h values can be larger.
- Dependency of M to the resolution N .
For the larger resolution 128^2 , there seems to be a dependency of M to the resolution N , however there's not a clear significance given

2.4.2 Studies for varying h and M : refined h & N

(benchmark: 2015_09_07_search_h_M_finite_differences_2)

Based on the previous results, we continue with additional parameter studies, but with h refined around the optimum interval $\{0.1, 0.2, \dots, 2.0\}$ and with larger resolutions to determine if there's a dependency of M to the resolution.

Note the different scaling for the coloring which we did for sake of clarity!



Here, we can observe indeed the requirement of M to be increased if also a decrease in error should be obtained. There also seems to be a linear dependence of M to the resolution N .

2.4.3 Conclusion

When using a finite-difference solver or any other solvers based on 1st order accurate approximations of the solution (e.g. finite-element with 1st order basis functions), this requires a dependency of M on the resolution N . We use the subindex to differentiate this determination of M to the one for a spectral solver.

$$M_{FD} := \frac{dt C_{FD}(e) N}{h\epsilon}. \quad (5)$$

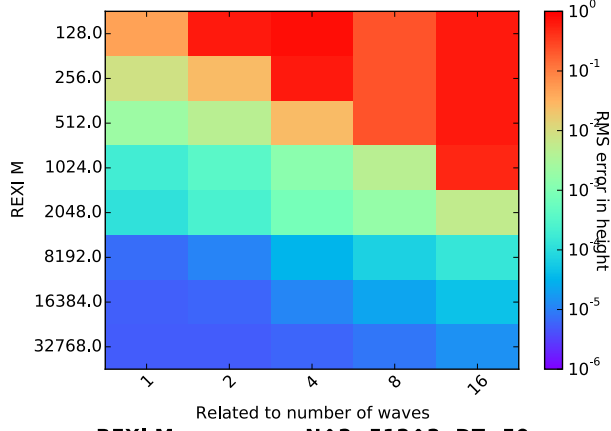
We should emphasize, that here the desired accuracy specified by e may be not achieved due to space-discretization errors. Finally we mention that the $C(e)$ already included the accuracy, hence this formula for determining M can be rewritten by making C dependent on N .

2.5 Dependency of M on number of waves W in initial conditions

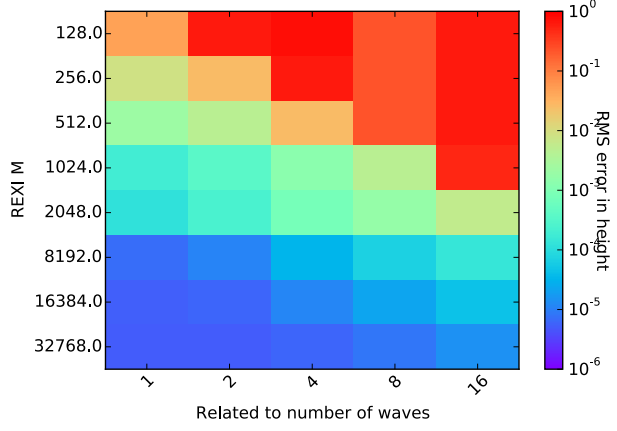
The REXI approach approximates the linear operator L acting on initial conditions. Hence, this approximation has to be able to capture all waves in the initial condition. Therefore, we next evaluate the possible dependency M on the number of frequencies in the initial condition (see Section 1.3.3). We briefly like to mention, that we skipped showing the resolutions 32^2 and 64^2 here, since all frequencies of the initial conditions cannot be captured by the grid resolution. We evaluated these studies with $h := 0.8$. Smaller values of h only resulted in a decrease of accuracy for a fixed M .

2.5.1 Spectral REXI:

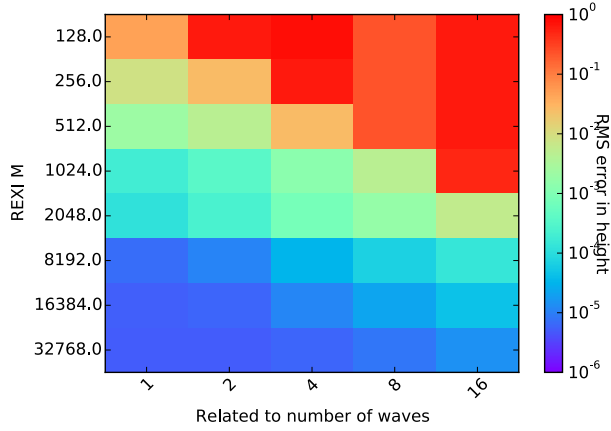
The simulation is executed over $DT := 50$ with $dt := 5$.
REXI M vs. waves, $N^2=128^2$, DT=50



REXI M vs. waves, $N^2=256^2$, DT=50



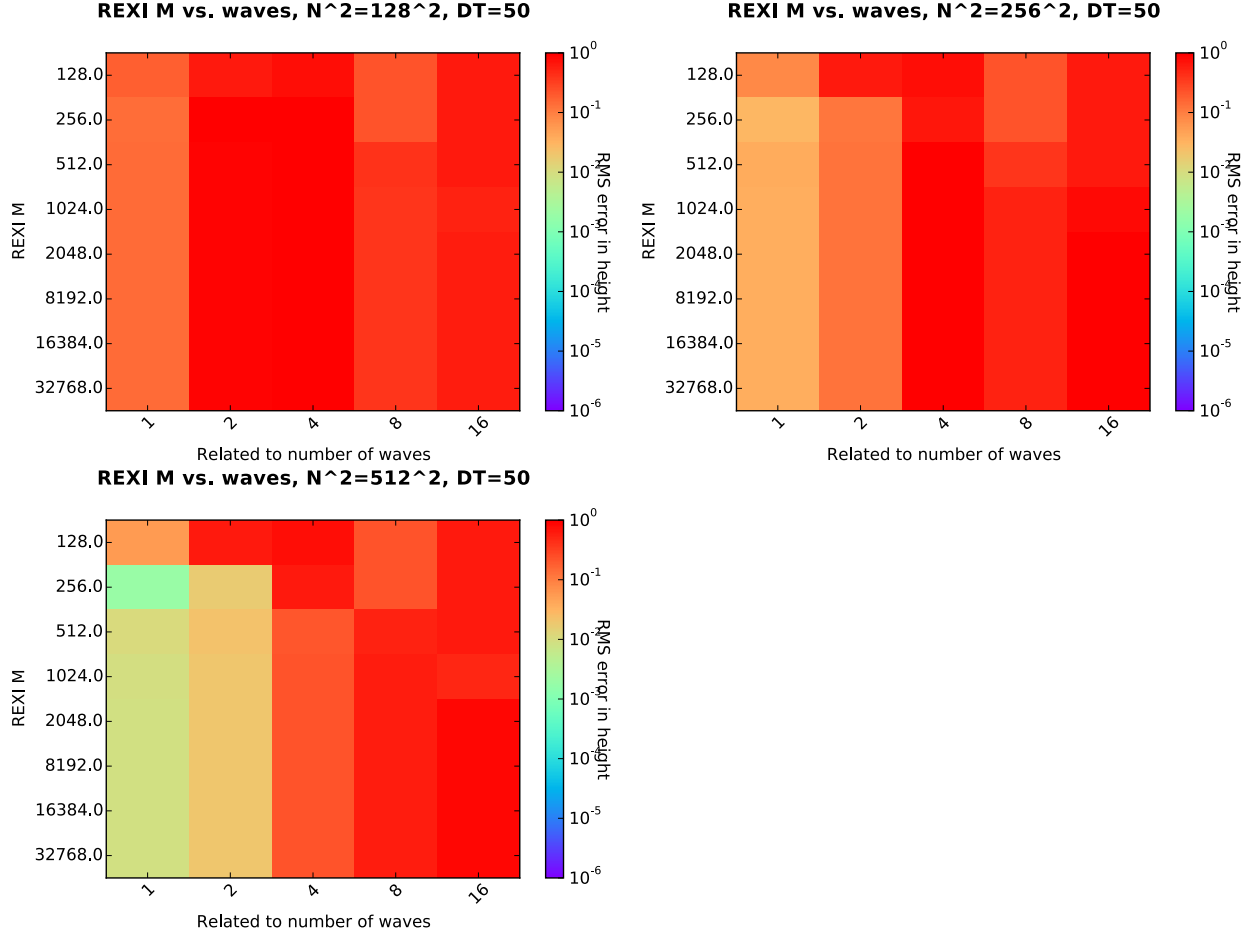
REXI M vs. waves, $N^2=512^2$, DT=50



We can observe, that for an increase of frequencies in the initial conditions (related to W), also an increase of the number of poles M for the REXI approximation is required in spectral space. The apparent independence of M to the resolution was already discussed in a previous Section which we expect to be dependent by using finite differences which we evaluate next.

2.5.2 Finite-difference REXI

We evaluate the accuracy and dependence of M on the resolution N and the number of waves W .



The accuracy of these simulations are significantly worse than the ones with the spectral solver. We like to mention, that we executed these studies over a very large time step size of $DT := 50$ which leads to these high inaccuracies. We can observe, that in these benchmarks, the parameter M also depends on the number of waves.

2.5.3 Conclusion

The number of poles for the REXI approximation depends on the frequencies in the solution. Since these frequencies are in general not known for arbitrary simulation states (assuming that a Fourier transformation is not feasible), the parameter M **has to be set to capture also the highest frequencies W** .

3 Performance benchmarks and comparison to standard time stepping schemes

Here, we compare the REXI approach with several other possible discretizations, see Sec. 1.5.

3.1 Performance studies for time stepping methods

(benchmark: 2015_09_16_performance_and_scalability_snbc)

We executed performance studies on a 16-core Intel Sandybridge system (2 sockets, each socket has 8 cores) to compare the overall computation time of several discretization methods with the REXI approach in both accuracy and time to solution. For initial conditions, we used the Gaussian distribution which generates frequencies over the entire band in Fourier space.

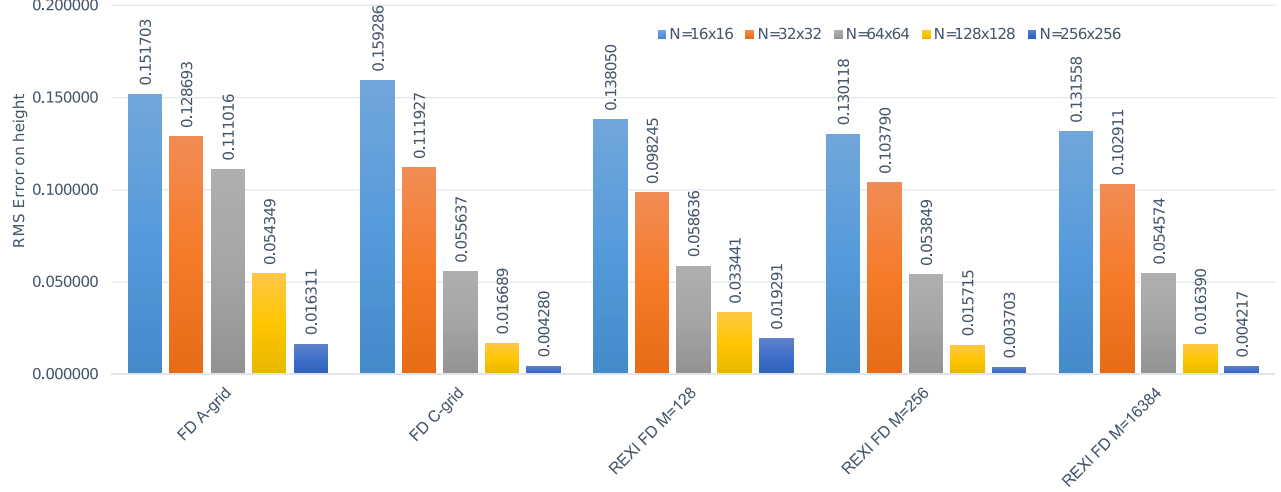
The initial conditions are given by the Gaussian distribution (see Sec. 1.3). For the non-REXI approaches, we use a $CFL := 0.3$ and RK4 time stepping method. For the approximated solution with REXI, a time step size of

$dt := 5$ is used. All simulations were executed over $DT := 50$ simulation seconds.

3.2 Error

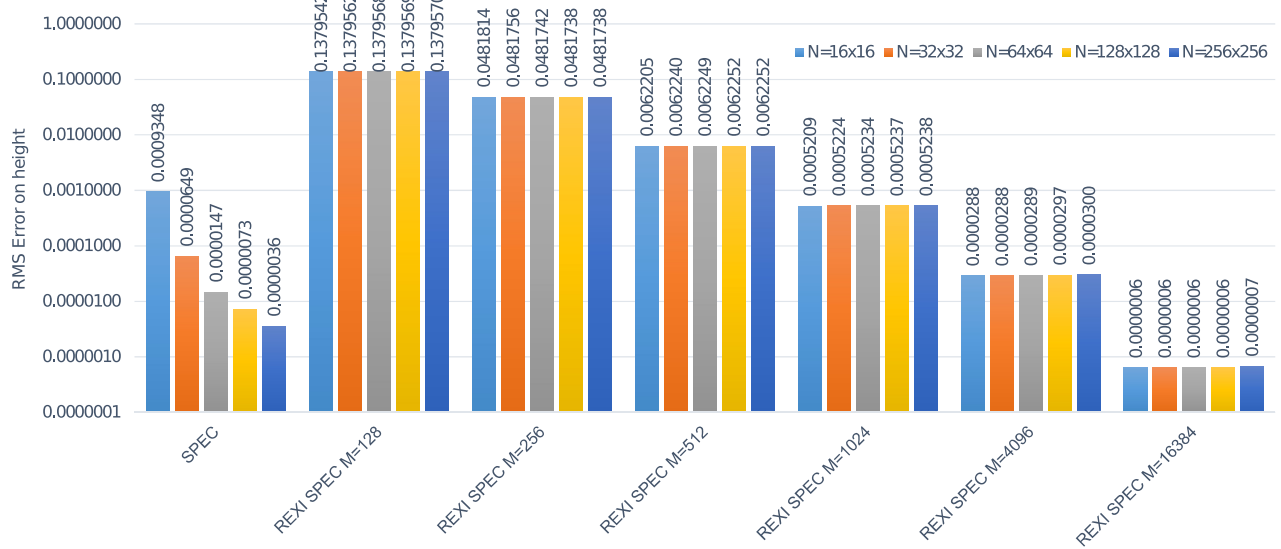
We first evaluate the errors for different time stepping methods, including REXI to compare the performance of similar results.

The following plot shows the results for the finite difference space discretization:



We can observe, that error with the REXI approach and with $M=256$ poles are competitive to the finite-difference results.

The next plot shows the accuracy for spectral discretization in space:



As we can see, only with about $M := 16384$, the REXI approximation is competitive to the standard spectral method.

3.3 Parallel performance

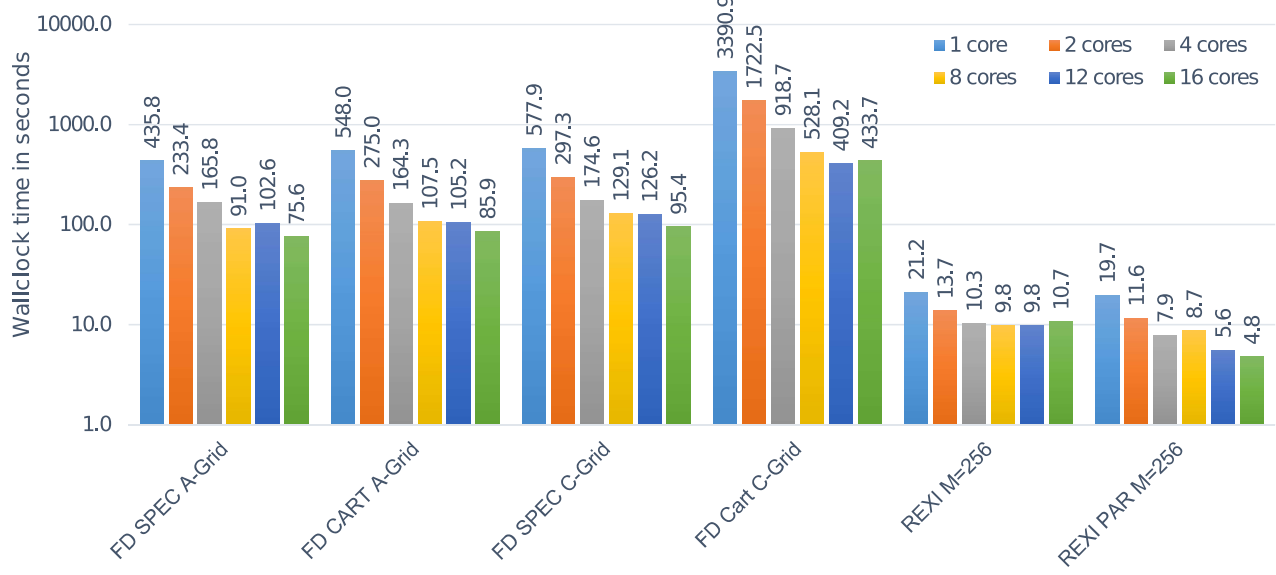
Regarding the parallelization, We tested two different parallelization concepts for the REXI method:

- REXI standard: The first one is the default one which parallelizes over the different solvers
- REXI PARSUM: The second one uses a parallelization over the sum and computes each term in the sum using only a single core.

For sake of reproducibility, we like to mention that we only discuss the results in this section based on memory allocator version 2 (in SWEET development) which resulted in the best results. This is a NUMA-aware memory allocator, avoids allocations on the heap and strongly improves the performance, hence allows a fair comparison of the computational amount. A solver in spectral space is used for solving the Helmholtz equation.

3.3.1 Finite-differences

We first have a look on the performance results for the finite difference method.



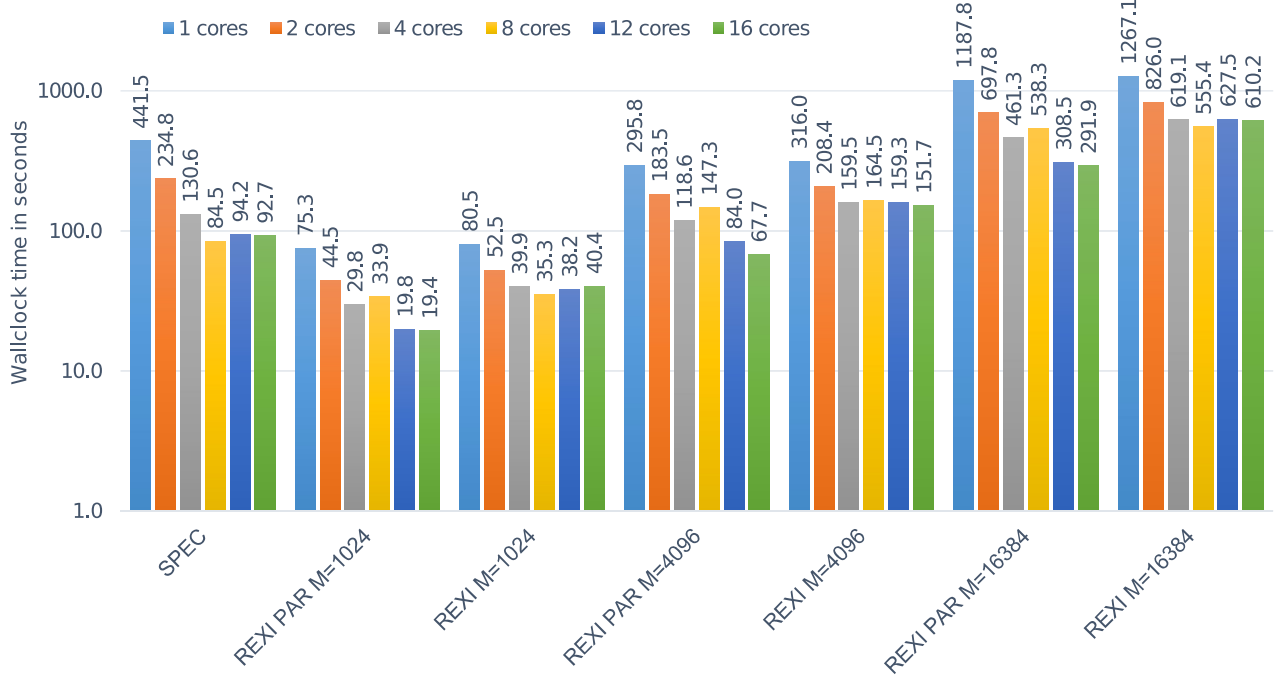
The axis for the wallclock time is in log scale. Comparing the REXI approach M=256 poles which obtains the same error bounds, we can observe speedups of (7.08, 8.04, 8.93, 40.62) compared to the standard time stepping methods from left to right in the performance results, respectively. We like to mention, that the FD method on the C-grid was not optimized. Therefore, we consider 8.93 as a realistic speedup.

Using a parallelization in space, we see a stagnating reduction in computation time in the 5 left-most groups of performance studies. With the REXI also a parallelization over the sum itself instead of a parallelization in space over the term in each sum is possible and denoted in the performance study above with “REXI PAR”. In contrast to the parallelization in space with its scalability limitation already reached (see REXI M=256) results, we can observe that there is still an increase in speedup of 1.81 by doubling the cores from 8 to 16 cores. Comparing both parallelization strategies, the REXI PAR implementation results in a speedup of 2.23.

To summarize, we achieve a speedup of 19.88 for problem sizes for which a speedup was not achievable with conventional parallelization-in-time methods.

3.3.2 Spectral space

Next, we evaluate possible speedup effects based on a spectral method used for the standard time stepping with RK4 with a parallelization-in-space:



Similar to the finite-difference method, we can observe a stagnation in the speedup for the parallelization-in-space. With the REXI approach, we would need $M := 16384$ poles to be competitive to the standard time stepping solver. Comparing the wallclock time with the best REXI PAR solver results in a speeddown of 3.15. We account for that by the super-convergence of the spectral solvers. However, as an outlook we should mention that the scalability of the REXI PAR implementation is not yet reached hence allows using even more cores.

4 Summary

[TODO]

5 Discussion of possible alternative approaches

5.1 Eigenvector decomposition in spectral space

Since the analytical solution is directly given by an Eigenvalue decomposition in spectral space, this could be an appropriate alternative to using the REXI approach. This is true for the f-plane. Let's analyze this property with the β -plane. Here, the f value is not constant over the plane, but varies depending on the y -coordinate:

$$f(y) := f_0 + \beta y$$

We can now have a look at the spectral formulation of the $L(U)$ operator

$$-L(U) := \begin{pmatrix} 0 & \eta_0 \partial_x & \eta_0 \partial_y \\ g \partial_x & 0 & -f(y) \\ g \partial_y & f(y) & 0 \end{pmatrix} U$$

with $U(\vec{x})$ given by its spectral superposition

$$U(\vec{x}) := \int_{\vec{k}} \tilde{U}(\vec{k}) e^{i\vec{k}\vec{x}}$$

and $f(\vec{x})$ given by

$$f(\vec{x}) := \int_{\vec{k}} \tilde{f}(\vec{k}) e^{i\vec{k}\vec{x}}.$$

We were able to compute the solution to $L(U)$ directly in spectral space with the EV decomposition, since we were able to factor out the spectral basis functions. An example is given here for the term $\eta_0 \partial_x$:

$$(\eta_0 \partial_x) \int_{\vec{k}} \tilde{U}(\vec{k}) e^{i\vec{k}\vec{x}} = \int_{\vec{k}} \tilde{U}(\vec{k}) \eta_0 \partial_x e^{i\vec{k}\vec{x}} = \int_{\vec{k}} \tilde{U}(\vec{k}) \eta_0 i \vec{k} e^{i\vec{k}\vec{x}} = \int_{\vec{k}} \tilde{U}(\vec{k}) (\eta_0 i \vec{k} e^{i\vec{k}\vec{x}})$$

In combination with a Ritz-Galerkin approach and using the orthogonality of the basis functions, this allows a wave-wise Eigenvalue decomposition. However for the $f(x)$ term, we are not able to factor out the basis function and apply the previously mentioned method

$$(f(y)) \int_{\vec{k}} \tilde{U}(\vec{k}) e^{i\vec{k}\vec{x}} = \int_{\vec{k}} f(\vec{k}) e^{i\vec{k}\vec{x}} \int_{\vec{k}} \tilde{U}(\vec{k}) e^{i\vec{k}\vec{x}}$$

which results in a non-linearity. Hence, we are not able to factor out the spectral basis functions and the approach is not applicable to the β -plane anymore.

References

- [1] Formulations of the shallow-water equations, M. Schreiber, P. Peixoto
- [2] High-order time-parallel approximation of evolution operators, T. Haut et al.
- [3] Understanding the Rational Approximation of the Exponential Integrator (REXI), Schreiber M., Peixoto P.
- [4] SWEET software development, <http://www.martin-schreiber.info/sweet/>, Schreiber M.